PNAS INAUGURAL ARTICLE | APPLIED MATHEMATICS OPEN ACCESS

Singularity formation in 3D Euler equations with smooth initial data and boundary

Jiajie Chen[a,1] and Thomas Y. Hou[b,1,2]

This contribution is part of the special series of Inaugural Articles by members of the National Academy of Sciences elected in 2024. Contributed by Thomas Y. Hou; received January 13, 2025; accepted May 20, 2025; reviewed by Russel E. Caflisch, Javier Gómez-Serrano, Vladimir Sverak, and Terence C. Tao

A long-standing fundamental open problem in mathematical fluid dynamics and nonlinear partial differential equations is to determine whether solutions of the 3D incompressible Euler equations can develop a finite-time singularity from smooth, finite-energy initial data. Leonhard Euler introduced these equations in 1757 [L. Euler, *Mémoires de l'Académie des Sci. de Berlin* 11, 274–315 (1757).], and they are closely linked to the Navier–Stokes equations and turbulence. While the general singularity formation problem remains unresolved, we review a recent computer-assisted proof of finite-time, nearly self-similar blowup for the 2D Boussinesq and 3D axisymmetric Euler equations in a smooth bounded domain with smooth initial data. The proof introduces a framework for (nearly) self-similar blowup, demonstrating the nonlinear stability of an approximate self-similar profile constructed numerically via the dynamical rescaling formulation.

Euler equations | singularity formation | computer-assisted proof | fluid dynamics

Significance

The problem of singularity formation of the 3D incompressible Euler equations with smooth initial data has remained open since Leonhard Euler introduced the equations in 1757. Beyond its importance in partial differential equations (PDE) analysis, the problem has drawn interest from physicists and engineers due to the potential impact of singularities on fluid flow modeling. This paper provides a rigorous solution of the problem for flows in a domain with a smooth boundary. It introduces a framework for studying nearly self-similar blowup, advancing our understanding of singularity formation not only in fluid mechanics but also in broader classes of nonlinear PDEs.

The three-dimensional (3D) incompressible Euler equations govern the motion of ideal incompressible fluids without external forcing in the inviscid setting. In the vorticity formulation, the Euler equations read

$$\omega_t + \mathbf{u}\cdot\nabla\omega = \omega\cdot\nabla\mathbf{u}. \quad \mathbf{u} = \nabla\times(-\Delta)^{-1}\omega, \qquad \textbf{[IE]}$$

where $\omega = \nabla\times\mathbf{u}$ is the vorticity vector and $\mathbf{u}$ is the velocity vector. These equations are among the most fundamental nonlinear partial differential equations (PDEs for short) with many important applications in science and engineering. Considerable effort has been devoted to studying the regularity properties of the 3D Euler equations; see, e.g., refs. 1 and 2. However, the fundamental questions concerning the global existence and regularity of solutions to these equations remain open and are widely regarded as among the most important in mathematical fluid mechanics.

Numerical simulations by Hou and Luo provide strong evidence for a finite-time singularity in the 3D axisymmetric Euler equations on the boundary of a periodic cylinder (3, 4). The singularity occurs at the intersection of the boundary $r = 1$ and the symmetry plane $z = 0$ (Fig. 1). Axisymmetry, the odd symmetry in the z direction, and the presence of the boundary all contribute to this blowup.

As illustrated in Fig. 1, the flow forms an antisymmetric pattern, with *Top* and *Bottom* swirls driving azimuthal flow toward the critical ring at $r = 1, z = 0$. This generates intense vorticity, disrupting the geometric regularity of the vorticity vector near $z = 0$ (6, 7), and leads to singularity formation at a hyperbolic saddle point (8). Several related studies (9–14) further support the Hou–Luo scenario as a strong candidate for an Euler singularity.

Recently, we have rigorously justified the Hou–Luo blowup scenario and established the following blowup result, summarized from refs. 15 and 16.

Theorem 1. *There exists a family of smooth initial data with finite energy such that the solution of the 3D axisymmetric Euler equations Eq.* ***IE*** *in the cylinder* $r, z \in [0,1]\times\mathbb{T}$ *develops a nearly self-similar singularity in finite time* T*, where* $\mathbb{T}$ *denotes the periodic torus.*

We develop a framework for (nearly) self-similar blowup by proving the stability of an approximate self-similar profile. Since the two-part paper is highly technical, we provide a high-level overview of the main ideas presented in refs. 15 and 16.

We remark that Elgindi and coauthors have proved a remarkable result that the 3D axisymmetric Euler equations in $\mathbb{R}^3$ with $C^{1,\alpha}$ velocity, for small α, and without swirl develop a finite-time singularity (17, 18). The weak regularity class with very small α is

Author affiliations: [a]Courant Institute of Mathematical Sciences, New York University, New York, NY 10012; and [b]Department of Computing and Mathematical Sciences, Caltech, Pasadena, CA 91125

Author contributions: J.C. and T.Y.H. designed research; J.C. and T.Y.H. performed research; J.C. contributed new reagents/analytic tools; J.C. and T.Y.H. analyzed data; and J.C. and T.Y.H. wrote the paper.

Reviewers: R.E.C., New York University; J.G.-S., Brown University; V.S., University of Minnesota Twin Cities Libraries; and T.C.T., University of California, Los Angeles.

The authors declare no competing interest.

Copyright © 2025 the Author(s). Published by PNAS. This open access article is distributed under Creative Commons Attribution License 4.0 (CC BY).

[1]J.C. and T.Y.H. contributed equally to this work.

[2]To whom correspondence may be addressed. Email: hou@cms.caltech.edu.

Published June 27, 2025.

Downloaded from https://www.pnas.org by Thomas Y.Z. Hou on June 27, 2025 from IP address 162.204.127.207.

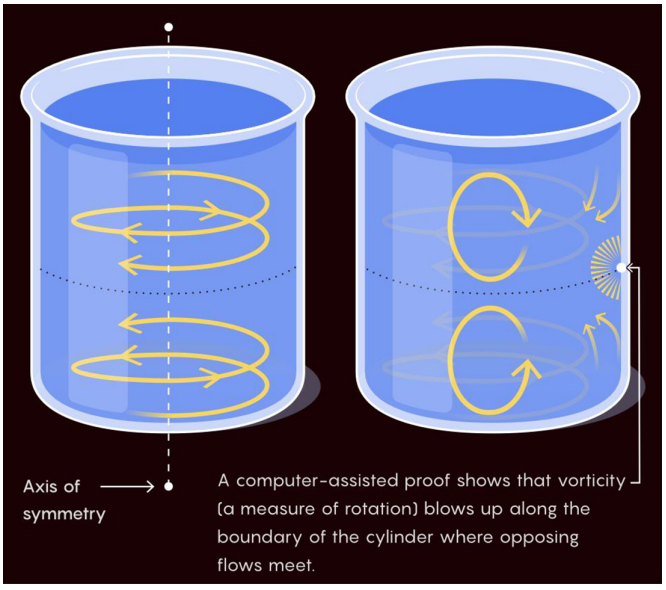

Fig. 1. An illustration of the flow structure in the Hou–Luo blowup scenario. Image Credit: Merrill Sherman/Quanta Magazine. Reprinted with permission from ref. 5.

essential in refs. 17 and 18. It is well known that the axisymmetric Euler equations without swirl have global regularity for smooth initial data (1). After our works (15, 16), finite-time blowup with $C^{1,\alpha}$ velocity and small α was constructed in ref. 19 for a new scenario and in ref. 20 using an iterative construction. Blowup with a solution-dependent force $f \in C^{1/2-}$ was established in ref. 21.

1.1. Difficulties. There are several difficulties in analyzing blowup in the 3D Euler equations with smooth data. First, advection induces a stabilizing effect that can deplete the singularity (22, 23). Second, the velocity $\mathbf{u} = \nabla \times (-\Delta)^{-1}\omega$ in Eq. **IE** depends nonlocally on the solution and is difficult to control. Third, the solution has a generic multidimensional structure.

In some previous works (13, 17, 24–26), the leading-order blowup profile can be reduced to a one-dimensional profile by imposing certain symmetry conditions. However, for the 3D Euler equations with smooth data, the incompressibility condition prevents such a reduction to a 1D PDE with small perturbations using natural symmetries. Thus, we must develop a new analytical method capable of handling the fully multidimensional problem.

1.2. Boundary. In the Hou–Luo scenario, the potential singularity forms at a stagnation point, where the boundary mitigates the effect of advection. Certain sign and symmetry properties generate a hyperbolic flow near the blowup point and enhance vortex stretching. Although advection normal to the boundary pushes fluid away-suppressing growth near the singularity-this effect vanishes at the boundary due to the no-flow condition. Thus, vortex stretching induces significant growth of vorticity near the boundary. This mechanism is captured by the Hou–Luo model along the boundary (27). In contrast, in a similar setting for 2D Boussinesq without a boundary, vorticity with odd symmetry in both x and y vanishes on $x = 0$ and $y = 0$, weakening vortex stretching relative to advection and thereby destroying the blowup mechanism.

2. A Framework for Nearly Self-Similar Blowup

To introduce our framework, we consider a general nonlinear PDE for a scalar function f

$$f_t = N(f), \qquad [1]$$

where $N(f)$ is a quadratic nonlinearity, such as f^2 or $f\partial_{ij}(-\Delta)^{-1}f$ for some $i,j \in \{1,2,3\}$, mimicking the vortex stretching term $\omega \cdot \nabla \mathbf{u}$ in Eq. **IE**.

We study a (nearly) self-similar blowup solution f to Eq. **1**, meaning that the solution maintains a similar pattern under suitable spatial rescaling and amplitude normalization. It can be described by:*

$$f(t,x) \approx \frac{1}{T-t}F(t, \frac{x}{(T-t)^{\mu(t)}}), \qquad ||F(t,\cdot) - \bar{F}||_X \ll 1\,, \qquad [2]$$

with some $\mu(t) > 0$, where $F(t,\cdot)$ remains close to an (approximate) blowup profile $\bar{F} \neq 0$ in some norm $||\cdot||_X$ uniformly up to the blowup time T.

To derive the equation for the rescaled solution F, we employ the dynamic rescaling formulation (28); see also ref. 29 for the related modulation technique. This approach dynamically and continuously rescales the physical solution both in space and time and in amplitude, according to certain normalization conditions. It yields an equivalent equation for F as follows

$$\partial_\tau F + c_l(\tau)\mathbf{x}\cdot\nabla F = N(F) + c_\omega(\tau)F, \qquad [3]$$

where the parameter $c_l(\tau)$ is used to zoom in on the blowup region, while $c_\omega(\tau)$ rescales the amplitude of the solution. The exponent μ in Eq. **2** is primarily determined by $|c_l(\tau)/c_\omega(\tau)|$. We can freely choose $c_l(\tau)$ and $c_\omega(\tau)$ to define Eq. **3**. An (approximate) steady state $\bar{F}$ of Eq. **3** corresponds to an (approximate) blowup profile $\bar{F}$ in Eq. **2**. Moreover, the blowup time $t = T$ maps to $\tau = \infty$ in the rescaled time. See Section 2.1.1 for the full transform in the case of the Boussinesq equations.

Our framework consists of three steps:

1. Construct the approximate steady state and blowup exponents $\bar{G} = (\bar{F}, \bar{c}_l, \bar{c}_\omega)$ to Eq. **3**;
2. Linearize the equations around $(\bar{F}, \bar{c}_l, \bar{c}_\omega)$ to obtain the perturbation equation for $\widetilde{G} = (F(\tau)-\bar{F}, c_l(\tau)-\bar{c}_l, c_\omega(\tau)-\bar{c}_\omega)$:

$$\partial_\tau \widetilde{G} = \mathcal{L}\widetilde{G} + \mathcal{N}(\widetilde{G}) + \mathcal{R}(\bar{G}), \qquad [4]$$

where $\mathcal{L}, \mathcal{N}, \mathcal{R}$ are the linear terms, nonlinear terms, and residual error, respectively. We then establish nonlinear stability estimates for a certain energy $E(\tau)$ of the perturbation $\widetilde{G}$, such as

$$\frac{d}{d\tau}E(\tau) \le -\lambda E(\tau) + CE(\tau)^2 + \varepsilon, \quad \lambda > 0, \qquad [5a]$$

where $-\lambda E$, CE^2, and ε estimate the contributions from the linear term, nonlinear term, and the residual error of the approximate steady state $\bar{F}$, respectively. Using a bootstrap argument, we can obtain nonlinear stability $E(\tau) < E^*$ for

*In general, the blowup rate in front of F depends on the nonlinearity $N(f)$ in Eq. **1**. Here, we adopt the blowup rate $\frac{1}{T-t}$, consistent with that of ω in Eq. **6**, and focus on this case for clarity.

Downloaded from https://www.pnas.org by Thomas Y.Z. Hou on June 27, 2025 from IP address 162.204.127.207.

some threshold $E^* \ll 1$ if ε is sufficiently small. For example, the condition

$$\varepsilon < \lambda^2/(4C) \quad \textbf{[5b]}$$

is sufficient to close Eq. **5**. This justifies $||F - \bar{F}||_X \ll 1$ in the ansatz Eq. **2**.

3. Construct the initial data with desired properties by perturbing the profile $\bar{F}$. Then, we construct a nearly self-similar blowup solution to Eq. **1** using the transform between Eq. **1** and Eq. **3**. Note that to prove blowup, we do not need to show that the solution F to Eq. **3** converges to an exact profile.

We first developed the above framework with Huang in refs. 27 and 30 for some 1D models of 3D Euler equations.

2.1. Dependency Tree of the Proof. *Theorem* 1 is proved using nonlinear stability estimates and inequalities similar to Eq. **5**, which rely on the three main components in the dependency tree. The most difficult part is establishing linear stability, i.e., $\lambda > 0$ in Eq. **5a**. We will discuss in some detail the key ideas behind sharp Hölder estimates in Section 3.4.2, finite-rank perturbations in Section 3.5.1, and linear energy estimates in Sections 3.1.1 and 3.2.1. In addition, we will briefly outline the approaches for estimating nonlocal terms in Section 4.3, nonlinear estimates in Section 3.7.1, constructing the profile in Section 4.1, estimating the profile and residual error in Section 4.2, and performing computer-assisted estimates (not shown in the dependency tree) in Section 3.7.2.

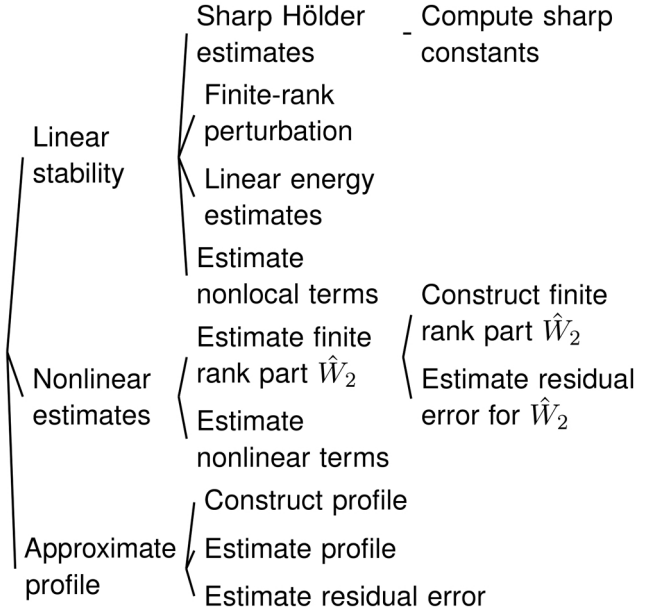

We refer to the more comprehensive dependency tree in 16, section 2.3, which illustrates how each part of the analysis maps to specific sections in refs. 15 and 16.

2.1.1. Dynamic rescaling formulation. The 3D axisymmetric Euler equations near the singularity (3) (located on the boundary away from the symmetry axis) can be formally approximated by the 2D Boussinesq (1, 13):

$$\partial_t \omega + \mathbf{u} \cdot \nabla \omega = \theta_x, \quad \textbf{[6a]}$$

$$\partial_t \theta + \mathbf{u} \cdot \nabla \theta = 0, \quad \mathbf{u} = \nabla^\perp (-\Delta)^{-1} \omega, \quad \textbf{[6b]}$$

in the upper half-space $(x, y) \in \mathbb{R}^2_+$ with the no-flow boundary condition $v(x, 0) = 0$, where $\mathbf{u} = (u, v)$ is the velocity, $\omega = u_y - v_x$ is the vorticity, and θ is the density or temperature. It is easy to show that

$$\widetilde{\omega}(\tau, \mathbf{x}) = C_\omega(\tau)\omega(t(\tau), C_l(\tau)\mathbf{x}),$$
$$\widetilde{\theta}(\tau, \mathbf{x}) = C_\omega^2(\tau) C_l(\tau)^{-1} \theta(t(\tau), C_l(\tau)\mathbf{x}),$$

solve the dynamic rescaling equations

$$\begin{aligned} \widetilde{\omega}_\tau + (c_l(\tau)\mathbf{x} + \widetilde{\mathbf{u}}) \cdot \nabla \widetilde{\omega} &= c_\omega(\tau)\widetilde{\omega} + \widetilde{\theta}_x, \\ \widetilde{\theta}_\tau + (c_l(\tau)\mathbf{x} + \widetilde{\mathbf{u}}) \cdot \nabla \widetilde{\theta} &= (c_l(\tau) + 2c_\omega(\tau))\widetilde{\theta}, \end{aligned} \quad \textbf{[7]}$$

where $\widetilde{\mathbf{u}} = (\widetilde{u}, \widetilde{v})^T = \nabla^\perp(-\Delta)^{-1}\widetilde{\omega}$, $\mathbf{x} = (x, y)^T$, τ is the rescaled time, $c_l(\tau)$, $c_\omega(\tau)$ are time-dependent scaling parameters, and $t(\tau) = \int_0^\tau C_\omega(\tau) d\tau$,

$$C_\omega(\tau) = e^{\int_0^\tau c_\omega(s) d\tau}, \quad C_l(\tau) = e^{\int_0^\tau -c_l(s) ds}. \quad \textbf{[8]}$$

Eq. **7** corresponds to Eq. **3**. To simplify our presentation, we still use t to denote the rescaled time τ and simplify $\widetilde{\omega}, \widetilde{\theta}$ as ω, θ. Eq. **7** becomes

$$\begin{aligned} \omega_t + (c_l\mathbf{x} + \mathbf{u}) \cdot \nabla \omega &= \theta_x + c_\omega \omega, \\ \theta_t + (c_l\mathbf{x} + \mathbf{u}) \cdot \nabla \theta &= (c_l + 2c_\omega)\theta. \end{aligned} \quad \textbf{[9]}$$

We impose normalization conditions on c_ω, c_l:

$$c_l(t) = 2\frac{\theta_{xx}(t, 0)}{\omega_x(t, 0)}, \quad c_\omega(t) = \frac{1}{2}c_l(t) + u_x(t, 0). \quad \textbf{[10]}$$

For smooth data, these two conditions enforce

$$\theta_{xx}(t, 0) = \theta_{0,xx}(0), \quad \omega_x(t, 0) = \omega_{0,x}(0), \quad \textbf{[11]}$$

for all time. We close the Eqs. **9** and **10**.

Following the blowup framework in Section 2, we aim to construct the approximate blowup profile $(\bar{\omega}, \bar{\theta}, \bar{c}_\omega, \bar{c}_l)$ for Eq. **9** and show that the perturbation $\tilde{G} = (\omega(t) - \bar{\omega}, \theta(t) - \bar{\theta}, c_\omega(t) - \bar{c}_\omega, c_l(t) - \bar{c}_l)$ remains small in some energy functional $E(\cdot)$: $E(\tilde{G}(t)) \ll 1$ for any $t \geq 0$. With this stability estimate and the values of the approximate scaling parameters $\bar{c}_l, \bar{c}_\omega$, the blowup asymptotics of the vorticity follow the form Eq. **2** with

$$F \approx \bar{\omega}, \quad \mu(t) \approx 2.92.$$

3. Key Methods in the Stability Estimates

The most difficult step is establishing the linear stability of the approximate profile. While refining the computation can yield a small residual error, e.g., ε in Eq. **5**, ε is not an arbitrarily small parameter, and obtaining a very small ε is highly challenging. To close the nonlinear estimates Eq. **5**, we must therefore develop quantitative and effective stability estimates with computable constants (e.g., λ, C in Eq. **5**).

A major challenge lies in controlling a compact operator arising from the nonlocal terms. A key distinction between our quantitative estimates of this compact operator (15, 16) (Section 3.5.1) and existing methods-such as finite codimension stability estimates (24, 31–34)-is that the latter rely on functional analysis and compactness arguments, resulting in implicit, uncomputable constants that cannot be used to close the argument in Eq. **5b**. In refs. 24 and 31–34, exact self-similar profiles (corresponding to $\varepsilon = 0$ in Eq. **5**) are constructed so that one does not need computable constants to close nonlinear estimates similar to Eq. **5b**.

Downloaded from https://www.pnas.org by Thomas Y.Z. Hou on June 27, 2025 from IP address 162.204.127.207.

3.1. Linearized Equations. Linearizing Eq. **9** around the approximate steady state and neglecting nonlinear and residual error terms yield the linearized equations for the perturbation $(\tilde{\omega}, \eta, \xi) \equiv (\omega - \bar{\omega}, \theta_x - \bar{\theta}_x, \theta_y - \bar{\theta}_y)$

$$\begin{aligned}\partial_t\omega + (\bar{c}_l x + \bar{\mathbf{u}}) \cdot \nabla\omega &= \eta + \bar{c}_\omega\omega \\ &\quad -\mathbf{u} \cdot \nabla\bar{\omega} + c_\omega\bar{\omega}, \qquad \textbf{[12a]}\\ \partial_t\eta + (\bar{c}_l x + \bar{\mathbf{u}}) \cdot \nabla\eta &= (2\bar{c}_\omega - \bar{u}_x)\eta - \bar{v}_x\xi \\ &\quad -\mathbf{u}_x \cdot \nabla\bar{\theta} - \mathbf{u} \cdot \nabla\bar{\theta}_x + 2c_\omega\bar{\theta}_x, \qquad \textbf{[12b]}\\ \partial_t\xi + (\bar{c}_l x + \bar{\mathbf{u}}) \cdot \nabla\xi &= (2\bar{c}_\omega + \bar{u}_x)\xi - \bar{u}_y\eta \\ &\quad -\mathbf{u}_y \cdot \nabla\bar{\theta} - \mathbf{u} \cdot \nabla\bar{\theta}_y + 2c_\omega\bar{\theta}_y, \qquad \textbf{[12c]}\end{aligned}$$

where $\mathbf{u} = (u, v) = \nabla^\perp(-\Delta)^{-1}\omega$, and $c_\omega = u_x(t, 0)$ by linearizing Eqs. **10** and **11**. Here, we abuse the notation ω to represent the perturbation $\tilde{\omega} = \omega - \bar{\omega}$.

3.1.1. Properties of the profile. The approximate profile we constructed satisfies the following properties with some constants $\kappa, \mu, \gamma, M_k > 0$.

(P1) Symmetries: $\bar{\theta}(x, y), \bar{v}(x, y)$ are even in x, $\bar{\omega}(x, y), \bar{u}(x, y)$ are odd in x, and $\nabla\bar{\theta}(0) = 0$.

(P2) Sign properties and scaling :

$$\mu \triangleq \bar{c}_l + \bar{u}_x(0) = 2\bar{c}_\omega - \bar{u}_x(0) > 0, \qquad \textbf{[13a]}$$

$$\bar{u}_x(0) < 0, \quad \bar{c}_l > 0, \quad \bar{c}_\omega < -0, \quad -\bar{c}_l/\bar{c}_\omega > 2. \qquad \textbf{[13b]}$$

(P3) Outflow flows: For any $x, y \geq 0$, we have

$$\bar{c}_l x + \bar{u}(x, y) \geq \kappa x, \quad \bar{c}_l y + \bar{v}(x, y) \geq \kappa y; \qquad \textbf{[13c]}$$

(P4) Decay conditions: For $k \leq 2$, we have

$$\begin{aligned}|\nabla^k\bar{\omega}| &\leq M_k \min(1, |\mathbf{x}|^{-\gamma-k}),\\ |\nabla^{k+1}\bar{\theta}| &\leq M_k \min(1, |\mathbf{x}|^{-2\gamma-k}),\\ |\nabla^k\bar{\mathbf{u}}| &\leq M_k \min(1, |\mathbf{x}|^{1-\gamma-k}).\end{aligned} \qquad \textbf{[13d]}$$

Let us explain property (P2). The condition $\bar{c}_l > 0$ indicates that the blowup is focusing, while $\bar{c}_\omega < 0$ implies finite-time blowup: $t(\infty) < \infty$ from Eq. **8**. Moreover, the condition $-\bar{c}_l/\bar{c}_\omega > 2$ follows from the conservation of $||\theta||_{L^\infty}$ in the 2D Boussinesq equations Eq. **6b**. The second identity in Eq. **13a** is a consequence of the normalization condition Eq. **10**.

3.2. Stability Mechanism. The outflow property Eq. **13c** for the transport coefficients in Eq. **12** plays a crucial role in establishing stability; see *Lemma* 2. It transports perturbations from the origin $\mathbf{x} = 0$ to the far field. In addition, the decay condition Eq. **13d** and the sign condition $\bar{c}_\omega < 0$ from Eq. **13a** imply that the system Eq. **12** is stable in the far field. These features form the core stability mechanisms of Eq. **12**. We use them to prove stability (i.e., $\lambda > 0$ in Eq. **5b**) for the operator $\mathcal{L}_0 = \mathcal{L} - \mathcal{K}_n$, where $\mathcal{L}$ is the linearized operator in Eq. **12** and $\mathcal{K}_n$ is a finite-rank perturbation. The operator $\mathcal{K}_n$ may introduce finitely many unstable eigenvalues to the full operator $\mathcal{L}$.

We do not know a priori whether $\mathcal{L}$ Eq. **12** is fully stable or stable modulo finitely many unstable directions. Even for simpler equations, such as the Burgers equation (35) or semilinear heat equation, some blowup profiles exhibit full stability while others are stable up to finitely many unstable modes.

In the Hou–Luo scenario, it was shown in ref. 36, section 3.4 that a discretized version of the linearized operator in a suitable finite-dimensional basis possesses a spectral gap. Moreover, our numerical results suggest that the blowup profile is not sensitive to perturbations in the initial data, as long as the initial data satisfy certain sign and symmetry conditions. To extend stability from $\mathcal{L} - \mathcal{K}_n$ to the full operator $\mathcal{L}$, we apply the approach in Section 3.5.1, which implicitly leverages these numerical observations.

3.2.1. Stability of the linearized operator with finite-rank perturbation. In this section, we discuss the method to show that the linearized operator Eq. **12** is stable in some suitable weighted space up to some finite-rank operator; see Eq. **25**.

To illustrate the key ideas for the stability estimates, we consider the following model problem

$$\partial_t f + \bar{V} \cdot \nabla f = \bar{a}(\mathbf{x})f + \bar{b}(\mathbf{x})B(f), \quad \bar{V} = \bar{c}_l\mathbf{x} + \bar{\mathbf{u}}, \qquad \textbf{[14]}$$

where $\nabla \cdot \bar{\mathbf{u}} = 0$ and $\bar{V}$ satisfies the sign and outflow properties Eqs. **13a–13c**

$$\bar{u}_x(0) < 0, \quad \bar{c}_l + \bar{v}_y(0) > \bar{c}_l + \bar{u}_x(0) = \mu > 0. \qquad \textbf{[15]}$$

The definition of μ is consistent with Eq. **13a**. The term $\bar{a}(x)f$ captures the diagonal part on the right side of Eq. **12**: $\bar{c}_\omega\omega$, $(2\bar{c}_\omega - \bar{u}_x)\eta$, or $(2\bar{c}_\omega + \bar{u}_x)\xi$, and we consider three cases of $(f, \bar{a})$:

$$(f, \bar{a}) = (\omega, \bar{c}_\omega), (\eta, 2\bar{c}_\omega - \bar{u}_x), \text{ or } (\xi, 2\bar{c}_\omega + \bar{u}_x). \qquad \textbf{[16]}$$

The coefficients $\bar{a}(\mathbf{x})$, $\bar{b}(\mathbf{x})$ satisfy the decay property

$$\begin{aligned}|\nabla^k\bar{b}(\mathbf{x})|,\ |\nabla^k(\bar{a}(\mathbf{x}) - \bar{a}(\infty))| &\leq M_k \min(1, |\mathbf{x}|^{-\gamma-k}),\\ |\bar{b}(\mathbf{x})| &\leq M_0 \min(|\mathbf{x}|, |\mathbf{x}|^{-\gamma}),\end{aligned} \qquad \textbf{[17]}$$

for $k \leq 2$ with $\bar{a}(\infty) = \lim_{|\mathbf{x}|\to\infty} \bar{a}(\mathbf{x})$, and $B(f) = K_B * f$ is a 0-th order singular integral operator related to the velocity, e.g. $B(f) = \partial_{ij}(-\Delta)^{-1}f$, $K_B(z) = \partial_{ij}\log(z)$ for $i, j \in \{1, 2\}$. The nonlocal term $\bar{b}(\mathbf{x})B(f)$ models the leading order nonlocal terms $\mathbf{u}_x \cdot \nabla\bar{\theta}$ and $\mathbf{u}_y \cdot \nabla\bar{\theta}$ in Eqs. **12b** and **12c**,[†] where the coefficient $\nabla\bar{\theta}$ vanishes near the origin. Note that we do not require the coefficients to be small, nor do we assume that $\bar{a}$ is negative. To extract the damping part, we use the following weighted estimates:

$$\begin{aligned}&\partial_t(f\varphi) + \bar{V} \cdot \nabla(f\varphi)\\ &= (\bar{a}(\mathbf{x}) + \frac{\bar{V} \cdot \nabla\varphi}{\varphi}) \cdot (f\varphi) + \bar{b}(\mathbf{x})B(f)\varphi \qquad \textbf{[18]}\\ &\triangleq d(\varphi) \cdot (f\varphi) + \mathcal{B},\end{aligned}$$

with a singular weight φ to be determined.

3.2.1.1. Outflow property and the damping terms. We consider the following weight

$$\varphi = \varphi_s\hat{\varphi}^m, \quad \varphi_s = |\mathbf{x}|^\alpha + |\mathbf{x}|^\beta, \qquad \textbf{[19a]}$$

where the singular weight φ_s with $\alpha < 0, \alpha < \beta$ captures the asymptotics of the weights, $\hat{\varphi} \asymp 1$ is more regular, and $m > 0$. We choose α, β such that

$$\bar{a}(0) + \mu\alpha \leq -\lambda, \quad \bar{a}(\infty) + \bar{c}_l\beta \leq -\lambda\,, \qquad \textbf{[19b]}$$

[†] If $f = \eta$ or ξ, the nonlocal terms $\nabla\mathbf{u}$ depend on ω rather than f. Since the estimates can extend to the system of (ω, η, ξ) Eq. **12**, we assume that the nonlocal term only depends on f to simplify the model.

Downloaded from https://www.pnas.org by Thomas Y.Z. Hou on June 27, 2025 from IP address 162.204.127.207.

for some $\lambda > 0$, where μ is defined in Eq. **15**, $\bar{a}$ in Eq. **16**, and $\bar{a}(\infty) = \lim_{|\mathbf{x}|\to\infty} \bar{a}(\mathbf{x})$. See more discussions in Section 3.3.1 for this constraint on stability. We can use the outflow property Eq. **13c** and $\hat{\varphi}$ to generate arbitrarily large damping terms in a bounded region away from the origin.

Lemma 2. *Let $d(\varphi)$ be the coefficient defined in Eq. **18**. For any $0 < R_1 < R_2$, $D > 0$ and $0 < \lambda_2 < \lambda$, there exists smooth $\hat{\varphi} \asymp 1$ and $m > 0$ depending on R_1, R_2, D, λ_2 such that*

$$d(\varphi) \le -\lambda_2 - D\mathbf{1}_{R_1\le|x|\le R_2}.$$

The left side of Eq. **19b** captures the asymptotics of $d(\varphi)$ near the origin and in the far-field, respectively.

Proof: For fixed λ_2 and D, we only need to prove the lemma for R_1 sufficiently small and R_2 large.

We represent the coefficient $d(\varphi)$ in Eq. **18** as

$$\begin{aligned} d(\varphi) &= \bar{a} + \frac{\bar{V}\cdot\nabla\varphi}{\varphi} \\ &= m\frac{\bar{V}\cdot\nabla\hat{\varphi}}{\hat{\varphi}} + \Big(\bar{a}(x) + (\bar{V}\cdot x)\cdot\frac{\alpha|x|^{\alpha-2}+\beta|x|^{\beta-2}}{|x|^\alpha+|x|^\beta}\Big) \\ &= J_1 + J_2. \end{aligned} \quad \textbf{[20]}$$

We estimate J_2 for small $|x|$ and large $|x|$ differently. Near 0, using Eq. **13d** for $\bar{a}(x)$, we get

$$\begin{aligned} J_2 \le& a(0) + \bar{C}\min(|x|^{\beta-\alpha}, |x|, 1) \\ &+ (\partial_1\bar{V}_1(0)x_1^2 + \partial_2\bar{V}_2(0)x_2^2)\cdot\alpha|x|^{-2}, \end{aligned}$$

for some constant $\bar{C}$ depending on α, β in Eq. **19** and M_k Eq. **13d** but independent of m, which can vary from line to line.[‡] Since $\alpha < 0$ from Eq. **19** and $\partial_1\bar{V}_1(0), \partial_2\bar{V}_2(0) \ge \mu$ from Eqs. **14** and **15**, we get

$$\begin{aligned} J_2 &\le \bar{a}(0) + \mu\alpha + \bar{C}\min(|x|^{\beta-\alpha}, |x|, 1) \\ &\le -\lambda + \bar{C}\min(|x|^{\beta-\alpha}, |x|, 1), \end{aligned}$$

where we have used Eq. **19** in the last inequality. Similarly, using the decay of $\bar{a}$ from Eqs. **13d** and **19**, we obtain

$$\begin{aligned} J_2 &\le a(\infty) + \bar{c}_l\beta + \bar{C}\min(|x|^{\alpha-\beta}, |x|^{-\beta}, 1) \\ &\le -\lambda + \bar{C}\min(|x|^{\alpha-\beta}, |x|^{-\beta}, 1). \end{aligned}$$

For $\lambda_2 < \lambda$, optimizing the above estimates, there exists $0 < \bar{R}_1(\lambda_2) < \bar{R}_2(\lambda_2)$ such that

$$J_2 \le -\lambda_2 + \bar{C}\mathbf{1}_{\bar{R}_1\le|x|\le\bar{R}_2}. \quad \textbf{[21]}$$

Given any $R_1, R_2 > 0$ with $R_1 \le \bar{R}_1(\lambda_2), \bar{R}_2(\lambda_2) \le R_2$, we choose a radial weight $\hat{\varphi}$ that satisfies

$$\begin{aligned} &\hat{\varphi}(r) = 1,\ r \le \frac{R_1}{2}, \qquad \hat{\varphi}(r) = \frac{1}{2},\ r \ge 2R_2, \\ &\partial_r\hat{\varphi}(r) \le 0,\ r \ge 0, \qquad \partial_r\hat{\varphi}(r) < 0,\ R_1 \le r \le R_2. \end{aligned}$$

It follows $\frac{r\partial_r\hat{\varphi}}{\hat{\varphi}} \le -\lambda_3\mathbf{1}_{R_1\le r\le R_2}$ for some $\lambda_3 = \lambda_3(R_1, R_2) > 0$. Using this estimate and the outflow property Eq. **13c**, we obtain

$$\begin{aligned} &\bar{V}(x)\cdot x \ge \kappa|x|^2 = \kappa r^2, \\ &J_1 = m\frac{\bar{V}\cdot\nabla\hat{\psi}}{\hat{\psi}} = m\frac{\bar{V}\cdot x}{r^2}\cdot\frac{r\partial_r\hat{\psi}}{\hat{\psi}} \le -m\lambda_3\kappa\mathbf{1}_{R_1\le r\le R_2}. \end{aligned}$$

Plugging the above estimates in J_1 in Eq. **20**, and then using Eq. **21**, we prove

$$d(\varphi)(x) = J_1 + J_2 \le -\lambda_2 + (\bar{C} - m\lambda_3\kappa)\mathbf{1}_{R_1\le r\le R_2}.$$

Choosing m large enough, we prove the lemma. □

3.2.1.2. Nonlocal part. For the nonlocal part in Eq. **18**, we have

$$\mathcal{B} = \bar{b}(\mathbf{x})B(f\varphi) - \bar{b}(\mathbf{x})[B,\varphi](f) = \mathcal{B}_M(f) - \mathcal{B}_C(f), \quad \textbf{[22a]}$$

where $\mathcal{B}_C$ is the commutator

$$\begin{aligned} \mathcal{B}_C(f)(\mathbf{x}) &= \bar{b}(\mathbf{x})(B(f\varphi) - \varphi B(f)) \\ &= \bar{b}(\mathbf{x})\int K_B(\mathbf{x}-\mathbf{y})\Big(1 - \frac{\varphi(\mathbf{x})}{\varphi(\mathbf{y})}\Big)(f\varphi)(\mathbf{y})d\mathbf{y}. \end{aligned} \quad \textbf{[22b]}$$

A crucial observation is that the leading order nonlocal term $\mathcal{B}_M(f) = \bar{b}(\mathbf{x})B(f\varphi)$ depends only on the weighted variable $f\varphi$. Therefore, it can be estimated with constants that are independent of the weight φ. Since the coefficient $\bar{b}(\mathbf{x})$ vanishes near $\mathbf{x} = \mathbf{0}$ and decays for large $\mathbf{x}$ Eq. **17**, we know that $\bar{b}(\mathbf{x})$ is small in both regions. By leveraging the strong damping term from *Lemma* 2 within a bounded region $\mathbf{x} : |\mathbf{x}| \in [R_1, R_2]$ away from $\mathbf{0}$, we can treat $\bar{b}(\mathbf{x})B(f\varphi)$ as a small perturbation to the local damping term $d(\varphi)\cdot(f\varphi)$ in the L^∞ energy estimate.[§]

Since $\bar{b}(\mathbf{x})$ vanishes near $\mathbf{x} = \mathbf{0}$ and decays in the far field by Eq. **17**, and the weight φ Eq. **19** is singular only near $\mathbf{x} = \mathbf{0}$, $1 - \frac{\varphi(\mathbf{x})}{\varphi(\mathbf{y})}$ cancels one order of singularity in the kernel $K_B(\mathbf{x}-\mathbf{y})$. This allows us to show that the operator $\mathcal{B}_C$ is roughly one order more regular than f.[¶] For instance, if $f \in L^\infty$, then $\mathcal{B}_C(f)$ is log-Lipschitz in a suitable weighted space. Moreover, $\mathcal{B}_C(f)$ can be approximated by a finite-rank operator.

3.3. Finite-Rank Operator. One approach is to use a piecewise approximation

$$\mathcal{K}_{MN}(f)(\mathbf{x}) = \sum_{i\le M, j\le N}\chi_{ij}(\mathbf{x})\mathcal{B}_C(f)(\mathbf{x}_{ij}), \quad \textbf{[23a]}$$

where $\chi_{ij}(\mathbf{x}) \ge 0$ is some sufficiently smooth cutoff functions covering a domain $[0, R_1]\times[0, R_2]$

$$\sum\chi_{ij}(\mathbf{x}) = 1, \quad \mathbf{x}\in[0,R_1]\times[0,R_2], \quad \textbf{[23b]}$$

[‡] It is important that the constants $\bar{C}, M_k$ are not sensitive to the residual error ϵ in Eq. **5a**. See more discussion in Section 3.7.1.

[§] Specifically, suppose that $||B(f\varphi)||_{L^\infty} \le C_1||f\varphi||_{L^\infty}$, where C_1 is independent of $f\varphi$. The above argument yields $C_1|\bar{b}(\mathbf{x})| + d(\varphi)(\mathbf{x}) \le -c < 0$ uniformly in $\mathbf{x}$. Thus, in the L^∞ estimate-neglecting lower-order terms such as $\mathcal{B}_C$-if the maximum of $|f\varphi(\cdot,t)|$ is attained at $\mathbf{x}$, then $|f\varphi(\mathbf{x},t)|$ decays in t, implying linear stability, i.e., $\lambda > 0$ in Eq. **5**. The full estimate is carried out in Lagrangian coordinates; see ref. 15, lemmas A.1 and A.2.

[¶] When $\varphi(y)$ is very small, we still gain a factor $|x-y|$ in $K_C = K_B(\mathbf{x}-\mathbf{y})\big(1-\frac{\varphi(\mathbf{x})}{\varphi(\mathbf{y})}\big)$. From Eq. **19** and *Lemma* 2, we have $|\nabla\varphi(\mathbf{y})| \asymp |\nabla\varphi(\mathbf{z})|$ for any $|\mathbf{y}| \asymp |\mathbf{z}|$. If $|\mathbf{x}| \asymp |\mathbf{y}|$, then $|1-\frac{\varphi(x)}{\varphi(y)}| \lesssim \frac{|\nabla\varphi(\mathbf{y})|}{\varphi(\mathbf{y})}|\mathbf{x}-\mathbf{y}| \lesssim |\mathbf{x}-\mathbf{y}|\cdot\frac{1}{|\mathbf{y}|}$. When $|\mathbf{y}| \asymp |\mathbf{x}|$ is small, the singular factor $|\mathbf{y}|^{-1}$ is absorbed by the coefficient $\bar{b}(\mathbf{x})$ in Eq. **22b**, since $|\bar{b}(\mathbf{x})| \lesssim |\mathbf{x}|$ by Eq. **17**. If $|\mathbf{x}| \ll |\mathbf{y}|$ or $|\mathbf{y}| \ll |\mathbf{x}|$, then $K_B(\mathbf{x}-\mathbf{y})$ is not singular. The integral of K_C is estimated using the methods in Section 4.3 by rescaling $(\mathbf{x},\mathbf{y})$ to $(\hat{\mathbf{x}},\hat{\mathbf{y}})$ with $|\hat{\mathbf{x}}| \asymp 1$ and partitioning the region for $\hat{\mathbf{y}}$ into three regimes: $|\hat{\mathbf{y}}| \ll |\hat{\mathbf{x}}|$, $|\hat{\mathbf{y}}| \asymp |\hat{\mathbf{x}}|$, and $|\hat{\mathbf{x}}| \ll |\hat{\mathbf{y}}|$. See ref. 16, section 4 for details.

Downloaded from https://www.pnas.org by Thomas Y.Z. Hou on June 27, 2025 from IP address 162.204.127.207.

in the first quadrant and it is supported locally near $\mathbf{x}_{ij}$ with support size of order h, e.g., $\mathbf{x}_{ij} = (ih, jh)$ with $0 \le i \le \frac{R_1}{h}, 0 \le j \le \frac{R_2}{h}$. Each term $\mathcal{B}_C(f)(x_{ij})$ is a rank-one operator and can be expressed as follows

$$\chi_{ij}(\mathbf{x})\mathcal{B}_C(f)(\mathbf{x}_{ij}) = p_{ij}(\mathbf{x}) \int f q_{ij} d\mathbf{x},$$

for some function p_{ij}, q_{ij}. Since χ_{ij} has a support size of $O(h)$, we obtain using Eq. **23** that for $\mathbf{x} \in [0, R_1] \times [0, R_2]$

$$\begin{aligned} &|\mathcal{K}_{MN}(f)(\mathbf{x}) - \mathcal{B}_C(f)(\mathbf{x})| \\ &= |\sum_{ij} \chi_{ij}(\mathbf{x})(\mathcal{B}_C(f)(\mathbf{x}) - \mathcal{B}_C(f)(\mathbf{x}_{ij}))| \\ &\le C h^{\alpha} \|\mathcal{B}_C(f)\|_{\dot{C}^{\alpha}} \sum \chi_{ij}(\mathbf{x}), \end{aligned}$$

where we have used $|\mathbf{x} - \mathbf{x}_{ij}| \le Ch$ for $\mathbf{x} \in \mathrm{supp}(\chi_{ij})$ in the inequality. Since $\mathcal{B}_C(f)$ is about one order more regular than f, we further obtain

$$|\mathcal{K}_{MN}(f)(\mathbf{x}) - \mathcal{B}_C(f)(\mathbf{x})| \le C_{\alpha}(\varphi) h^{\alpha} \|f\varphi\|_{L^{\infty}}, \qquad [24]$$

for any $\alpha \in (0, 1)$, the constant $C_{\alpha}(\varphi)$ depends on the weight φ and α, but is independent of h. The approximation error is also small in the $C^{1/2}$ norm by choosing $\alpha > \frac{1}{2}$ and small h. For $\mathbf{x} \notin [0, R_1] \times [0, R_2]$ with R_1, R_2 suitably large, we gain smallness in the upper bound of Eq. **24** from the decay of $\bar{b}(\mathbf{x})$ in $\mathcal{B}_C$; see Eq. **22b**. By choosing R_1, R_2 and the rank M, N suitably large so that h is small, we can treat the approximation error $|\mathcal{K}_{MN}(f)(\mathbf{x}) - \mathcal{B}_C(f)(\mathbf{x})|$ perturbatively in the energy estimate.

Using the above method, we can establish exponential decay estimates of the linearized operator in some suitable weighted space up to a finite-rank operator

$$\partial_t f = (\mathcal{L} - \mathcal{K}_{MN}) f. \qquad [25]$$

We will discuss more on the construction of $\mathcal{K}_{MN}$ and the estimate of $\mathcal{K}_{MN}$ in Section 3.5.1.

3.3.1. Singularity and asymptotics of weights. Below, we discuss the condition Eq. **19b** for the weighted estimates of ω, η, ξ in the linearized equations Eq. **12**. One may choose weights as

$$\varphi_f = (|\mathbf{x}|^{\alpha_f} + |\mathbf{x}|^{\beta_f})\hat{\varphi}^m, \quad f = \omega, \eta, \xi. \qquad [26]$$

Due to the decay and vanishing conditions of the coefficients in the off-diagonal local part in Eq. **12**—e.g., $\bar{v}_x$ in $\bar{v}_x \xi$ and $\bar{u}_y$ in $\bar{u}_y \eta$—we can treat these terms perturbatively for $|\mathbf{x}|$ very small or very large. Recall the definition of $\bar{a}(x)$ from Eq. **16**. We have $\bar{a}_{\eta}(x) = 2\bar{c}_{\omega} - \bar{u}_x$ in the η-equation and $\bar{a}_{\xi} = 2\bar{c}_{\omega} + \bar{u}_x$ in the ξ-equation. Using μ from Eq. **13a** (same as Eq. **15**) and the decay of $\bar{u}_x$ from Eq. **13d**, we obtain

$$\begin{aligned} &\bar{a}_{\eta}(0) = \mu, && \bar{a}_{\eta}(\infty) = 2\bar{c}_{\omega}, \\ &\bar{a}_{\xi}(0) = 4\bar{c}_{\omega} - \mu < 0, && \bar{a}_{\xi}(\infty) = 2\bar{c}_{\omega}. \end{aligned} \qquad [27]$$

Plugging Eq. **27** into Eq. **19b**, to design the weight φ_{η} for estimating $\eta\varphi_{\eta}$, we require

$$\begin{aligned} &\mu + \mu\alpha_{\eta} < 0, && 2\bar{c}_{\omega} + \bar{c}_l \beta_{\eta} < 0, \\ \Rightarrow\ &\alpha_{\eta} < -1, && \beta_{\eta} < -2\bar{c}_{\omega}/\bar{c}_l. \end{aligned} \qquad [28a]$$

Similarly, to design the weight φ_{ξ} for $\xi\varphi_{\xi}$, we require

$$\begin{aligned} &4\bar{c}_{\omega} - \mu + \mu\alpha_{\xi} < 0, && 2\bar{c}_{\omega} + \bar{c}_l \beta_{\xi} < 0, \\ \Rightarrow\ &\alpha_{\xi} < 1 - 4\bar{c}_{\omega}/\mu, && \beta_{\xi} < -2\bar{c}_{\omega}/\bar{c}_l. \end{aligned} \qquad [28b]$$

The variable ξ admits much better stability estimates. Recall the normalization conditions Eq. **11** on θ, which imply $\eta = O(|x|^2)$ and $\xi = O(|x|^2)$ near $\mathbf{x} = 0$. Thus, we can choose $a_{\eta} \le -2$ and $a_{\xi} < 0$ to satisfy the first condition in Eq. **19b**. Since $-\frac{2\bar{c}_{\omega}}{c_l} > 0$, we can select $\beta_{\eta}, \beta_{\xi} \in (0, -\frac{2\bar{c}_{\omega}}{c_l})$ to satisfy the second condition in Eq. **19b** and to capture the decay of η and ξ using these weights.

Although the coefficient 1 in the off-diagonal local term η in the ω-equation Eq. **12a** does not decay, we can still treat η perturbatively for $|\mathbf{x}|$ very small or very large by designing φ_{ω} in Eq. **26** for the ω-equation Eq. **12a** to be weaker than φ_{η}. We choose

$$\alpha_{\omega} - \alpha_{\eta} > 0, \quad \beta_{\omega} - \beta_{\eta} < 0. \qquad [28c]$$

Then the coefficient in the estimate

$$|\eta\varphi_{\omega}| \le \frac{\varphi_{\omega}}{\varphi_{\eta}} |\eta\varphi_{\eta}| \lesssim \min(|\mathbf{x}|^{\alpha_{\omega} - \alpha_{\eta}}, |\mathbf{x}|^{\beta_{\omega} - \beta_{\eta}}) |\eta\varphi_{\eta}|$$

is small for $|\mathbf{x}|$ very small or very large.

We now return to the constraint Eq. **19b**. For ω-equation Eq. **12a**, we have $\bar{a}_{\omega}(\mathbf{x}) = \bar{c}_{\omega}$ and require

$$\begin{aligned} &\bar{c}_{\omega} + \mu\alpha_{\omega} < 0, && \bar{c}_{\omega} + \bar{c}_l \beta_{\omega} < 0, \\ \Rightarrow\ &\alpha_{\omega} < -\bar{c}_{\omega}/\mu, && \beta_{\omega} < -\bar{c}_{\omega}/c_l. \end{aligned} \qquad [28d]$$

Note that the upper bound for β_{ω} is smaller than that for $\beta_{\eta}, \beta_{\xi}$, as given by Eqs. **28a** and **28b**. This indicates that we can choose $\varphi_{\eta}, \varphi_{\xi}$ with slower decay than φ_{ω} and obtain faster decay estimates for η, ξ than for ω. The first condition in Eq. **28d** holds for any $\alpha_{\omega} < 0$. It is straightforward to verify that the conditions in Eq. **28** hold for a wide range of $\alpha., \beta.$ with $\alpha. \ge -3$.

3.4. Same Velocity. In Eq. **12**, the velocity $\bar{c}_l \mathbf{x} + \bar{\mathbf{u}}$ is the same for all three equations. Thus, we can extract the outflow property using the same factor $\hat{\varphi}$ in Eq. **26**.

3.4.1. Weighted estimates in ref. 15. For the blowup profile, we have

$$-\bar{c}_{\omega}/\bar{c}_l \approx 0.34.$$

In ref. 15, we first perform weighted L^{∞} estimates with faster decay weights (see φ_i in ref. 15, appendix C)

$$\alpha_{\omega,\eta,\xi} = (-2.9, -3, -3),\ \beta_{\omega,\eta,\xi} = (-\frac{1}{6}, \frac{1}{7}, \frac{1}{7}), \qquad [29a]$$

where $\alpha_{\omega,\eta,\xi} = (\alpha_{\omega}, \alpha_{\eta}, \alpha_{\xi})$ and $\beta_{\omega,\eta,\xi} = (\beta_{\omega}, \beta_{\eta}, \beta_{\xi})$. We use a similar notation below in Eq. **29b**. To further bound ω, η, ξ in L^{∞}, we perform additional weighted L^{∞} estimates with growing weights (see $\varphi_{g,i}$, $i = 1, 2, 3$ in ref. 15, appendix C)

$$\begin{aligned} &\alpha^{\mathrm{gr}}_{\omega,\eta,\xi} = (-2.9, -3, -3), \\ &\beta^{\mathrm{gr}}_{\omega,\eta,\xi} = (\frac{1}{16}, \frac{1}{3} + 10^{-8}, \frac{1}{3} + 10^{-8}). \end{aligned} \qquad [29b]$$

The exponents in Eqs. **29a** and **29b** satisfy conditions Eq. **28** for stability. In ref. 15, instead of designing the weight using the formula from Eq. **19**, we use

$$\varphi = \sum_{i \le n} p_i |\mathbf{x}|^{\alpha_i}, \text{ or } \varphi = |x_1|^{-1/2} \sum_{i \le n} p_i |\mathbf{x}|^{\alpha_i}. \qquad [29c]$$

Downloaded from https://www.pnas.org by Thomas Y.Z. Hou on June 27, 2025 from IP address 162.204.127.207.

That is, we use a power function $|\mathbf{x}|^{\alpha_i}$ instead of $\hat{\varphi}^m$ for the regular part. These choices of weights allow us to obtain a stronger weight in the far-field and obtain better embedding constants (smaller C in Eq. **5**), e.g., $|\omega| \le \varphi^{-1}||\omega\varphi||_{L^\infty}$, to close the nonlinear estimates. Moreover, the explicit form in Eq. **29c** makes it easier to estimate the piecewise bounds of the weights.

3.4.2. Weighted $C^{1/2}$ estimates and optimal transport. Since the Riesz transform $\partial_{ij}(-\Delta)^{-1}$ associated with the nonlocal term (see the discussion below Eq. **17**) is not bounded in L^∞, we perform the weighted $C^{1/2}$ estimates in ref. 15 to close the estimates. We use ideas and methods similar to those in *Lemma* 2 and Section 3.2.1 to extract the damping terms and obtain weighted $C^{1/2}$ and L^∞ estimates of Eq. **12** up to a finite-rank operator Eq. **25**. To close nonlinear estimates with ϵ not extremely small (see constraint Eq. **5**), we aim to obtain a good bound on λ Eq. **5** for linear stability. For this purpose, we develop sharp $C^{1/2}$ estimates.

We have a key observation that the Hölder estimate of the nonlocal term with a sharp constant is related to an optimal transport problem. We focus on the main nonlocal term $\widetilde{u}_x$. In the C^α_x estimate[#] of $u_x(x,0) - u_x(z,0)$ with $\alpha \in (0,1)$, using the translation and scaling symmetries, we only need to estimate

$$\begin{aligned} S &= u_x(1/2,0) - u_x(-1/2,0) \\ &= -\frac{1}{\pi} P.V. \int_{\mathbb{R}^2} k(s)\omega(s_1,-s_2)ds, \end{aligned} \qquad [30]$$

in terms of $||\omega||_{\dot{C}^\alpha_x}$, with $\int k(s)ds = 0$. In a simpler example where $k(y) = \delta(y-1) + \delta(y-2) - \delta(y-3) - \delta(y-4)$, we have an optimal estimate

$$\begin{aligned} S = \left| \int k(y)f(y)dy \right| &\le |f(2) - f(3)| + |f(1) - f(4)| \\ &\le (1+3^\alpha)||f||_{\dot{C}^{1/2}}. \end{aligned}$$

It can be interpreted as moving the mass from 2 to 3 and 1 to 4 with the cost function $|x-y|^\alpha||f||_{\dot{C}^\alpha}$. In general, an estimate of S using $||\omega||_{\dot{C}^\alpha}$ is equivalent to estimating the transportation cost of moving the positive region of $k(y)$ with measure $k^+(y)dy$ to its negative region with measure $k^-(y)dy$ with the concave cost function $c(x,y) = |x-y|^\alpha$. Thus, to obtain a sharp estimate of S Eq. **30**, we seek a measurable transport map to obtain a cost as small as possible.

For more general 1D cases, we can derive the optimal estimate and the equation of the map:

Lemma 3. *[Transportation Lemma] Suppose there exists $c \in (a,b)$ such that $f < 0$ on (a,c), $f > 0$ on (c,b), $f|x-c|^\alpha \in L^1_{loc}$ with $\int_a^b f(x)dx = 0$. For $\alpha \in (0,1)$, $g \in C^\alpha(a,b)$, we have*

$$\left| \int_a^b f(x)g(x)dx \right| \le \int_c^b |f(x)||x - T(x)|^\alpha dx \cdot ||g||_{\dot{C}^\alpha},$$

where $T(x)$ solves $\int_x^{T(x)} f(s)ds = 0$.

Note that we have the same optimal map $T(x)$ for any $\alpha \in (0,1)$ since the cost function $|x|^\alpha$ is concave. The bound is given by some explicit integral depending on the map. To estimate Eq. **30**, we analyze the sign of $k(s_1,s_2)$ for each fixed s_2 and apply *Lemma* 3 horizontally to construct the transport map $T(s)$ in two dimensions, which solves a cubic equation.[‖] For any $\mathbf{x},\mathbf{z} \in \mathbb{R}^2_+$ with $x_2 = z_2$, we can obtain

$$|u_x(\mathbf{x}) - u_x(\mathbf{z})| \le C_*|x_1 - z_1|^{1/2}[\omega]_{C^{1/2}_x}, \qquad [31]$$

where $[\cdot]_{C^{1/2}_x}$ denotes the seminorm (see Footnote #). The explicit formula of C_* with $C_* \le 2.55$ and a stronger version of Eq. **31** were established in ref. 15, lemma 3.1.

We can develop similar sharp $C^{1/2}_x, C^{1/2}_y$ estimates (see Footnote #) for other terms in $\nabla\mathbf{u}$ using *Lemma* 3. Using the triangle inequality, we can combine the Hölder estimates in $\mathbb{R}^2_+$. We refer the details of these estimates to ref. 15, section 3 and appendix B.

We can generalize unweighted Hölder estimates to weighted ones with the same constant independent of the weight up to some more regular terms depending on the weight, like the commutator $\mathcal{B}_C$ in Eq. **22b**. Estimates of the more regular terms follow Section 4.3.

3.5. Main part in the energy. Based on the previous analysis, the main part of the energy (corresponding to E in Eq. **5**) consists of

$$\begin{aligned} E_M(f) &= \max\Big(\max_{i\le 3}||f_i\varphi_i||_{L^\infty}, \max_{i\le 3}||f_i\psi_i||_{C^{1/2}_{g_i}}\Big), \\ ||F||_{C^{1/2}_{g_i}} &= ||(F(\mathbf{x}) - F(\mathbf{y}))g_i(\mathbf{x}-\mathbf{y})||_{L^\infty(\mathbb{R}^2_+\times\mathbb{R}^2_+)}, \end{aligned}$$

for some singular weights φ_i, ψ_i, where $g_i(h) \asymp |h|^{-1/2}$ is $-\frac{1}{2}$-homogeneous and $||\cdot||_{C^{1/2}_{g_i}}$ is a seminorm equivalent to the $C^{1/2}$ seminorm. We modify $g_i(h)$ to explore the anisotropy of the flow $\bar{c}_I\mathbf{x} + \bar{\mathbf{u}}$. Since the $C^{1/2}$ estimate is akin to taking a half derivative, we design ψ_i to be $|x|^{1/2}$ more regular than φ_i near $x = 0$ (Eq. **29**) so that the energy E_M is well defined for $\omega, \eta, \xi = O(|x|^3)$ near $x = 0$. Additional norms are included in the energy to obtain sharper stability estimates. We refer the reader to the full energy formulation in ref. 15, section 2.2. The energy E_M is applied to control the first component of the perturbation, namely W_1, as discussed in Section 3.5.1.

In the weighted energy estimates, we must carefully estimate the associated coefficients-such as ratios between weights-and control the relevant variables in appropriate functional spaces. These steps lead to rather technical estimates, as detailed in ref. 15.

3.5.1. Finite-rank perturbation. In Section 3.2.1, we introduced methods for establishing the stability of the linearized Eqs. **14** and **25** with a finite-rank perturbation $\mathcal{K}_n$. In this section, we further develop the finite-rank perturbation framework to estimate $\mathcal{K}_n$.

We can rewrite the linearized equation Eq. **12** for $W = (\omega,\eta,\xi)$ schematically as $\partial_t W = \mathcal{L}W$. We decompose $W = W_1 + W_2$ with W_i solving

$$\begin{aligned} \partial_t W_1 &= (\mathcal{L} - \mathcal{K}_n)W_1, \\ \partial_t W_2 &= \mathcal{L}W_2 + \mathcal{K}_n W_1, \end{aligned} \qquad [32a]$$

using initial data $(W_1,W_2)|_{t=0} = (W|_{t=0}, 0)$, where $\mathcal{K}_n W_1 = \sum_{i\le n} a_i(W_1)\bar{g}_i$ is some finite-rank operator with given

[#] We refer to C^α_x estimate as estimating $|f(P) - f(Q)|/|P-Q|^\alpha$ for $P,Q \in \mathbb{R}^2_+$ with $P_2 = Q_2$ but $P_1 \ne Q_1$. We define C^α_y similarly and denote by $[f]_{C^\alpha_x}, [f]_{C^\alpha_y}$ the seminorms.

[‖] For fixed $\mathbf{x},\mathbf{z}$, we consider $K_\Delta(y) = K(\mathbf{x}-\mathbf{y}) - K(\mathbf{x}-\mathbf{z})$ with kernel K associated with the velocity operator $\partial_{ij}(-\Delta)^{-1}$. Using *Lemma* 3, we solve $T(a)$ from $\int_a^{T(a)} K_\Delta(y)dy_i = 0$ for $i = 1$ or $i = 2$, which reduces to a cubic equation of $T(a)$ when $x_1 = z_1$ or $x_2 = z_2$. Moreover, using translation and scaling symmetries in the Hölder estimate, we can reduce the pairs $(\mathbf{x},\mathbf{z})$ with $x_i = z_i$ depending on three parameters (e.g. x_1, z_1, x_2) to at most one parameter.

Downloaded from https://www.pnas.org by Thomas Y.Z. Hou on June 27, 2025 from IP address 162.204.127.207.

functions $\bar{g}_i$. We design $\mathcal{K}_n$ to approximate more regular nonlocal terms and to obtain exponential decay estimates of W_1 in some weighted norm X. See Section 3.2.1. Since W_2 has zero initial data, we represent it using Duhamel's formula

$$\begin{aligned} W_2(t) &= \int_0^t e^{\mathcal{L}(t-s)}\Big(\mathcal{K}_n W_1(s)\Big)ds \\ &= \sum_{i\le n}\int_0^t a_i(W_1(s))e^{\mathcal{L}(t-s)}\bar{g}_i ds. \end{aligned} \quad \textbf{[32b]}$$

The stability estimate for W_1 implies that $a_i(W_1(s))$ decays exponentially. If $e^{\mathcal{L}s}\bar{g}_i$ decays in the energy space X as $s\to\infty$, we can derive decay estimates for W_2 in X. It is important to note that the decay of $|e^{\mathcal{L}s}\bar{g}_i|_X$ for large s is not only sufficient but also necessary for the stability of $\mathcal{L}$ in X. This approach-obtaining the stability of an operator perturbed by a finite-rank operator $\mathcal{K}$ by testing decay on the modes in $\mathcal{K}$-is related to the Sherman–Morrison formula (37) in linear algebra, and the $T(1)$ (38) and $T(b)$ (39, 40) theorems in harmonic analysis.

Note that numerical evidence of linear stability of $\mathcal{L}$ defined in Eq. **12** with a spectral gap has been obtained by Liu (36). Thus, one would expect that $e^{\mathcal{L}s}\bar{g}_i$ decays for large s. Since we can design $\bar{g}_i$ and $\mathcal{L}$ is given, to verify the decay of $e^{\mathcal{L}s}\bar{g}_i$, we construct its space-time approximation by solving

$$\partial_t g = \mathcal{L}g, \quad g|_{t=0} = \bar{g}_i, \qquad \textbf{[33]}$$

numerically and using a numerical basis and a representation similar to Eq. **36**. By interpolating the numerical solution at discrete time t_k using a cubic polynomial in t, we construct an approximate space-time solution $\widehat{g}_i(t,\mathbf{x})$. To track the numerical error in solving the PDE, we use a posteriori error estimate and introduce the residual operator

$$\begin{aligned} \mathcal{R}(W_1,t) = \sum_{i\le n}\Big(&a_i(W_1(t))(\hat{g}_i(0,\mathbf{x})-\bar{g}_i) \\ &+\int_0^t a_i(W_1(t-s))(\partial_s-\mathcal{L})\hat{g}_i(s,\mathbf{x}))ds\Big), \end{aligned} \quad \textbf{[34a]}$$

and modify the representation of W_2 as follows

$$\widehat{W}_2 = \sum_{i\le n}\int_0^t a_i(W_1(t-s))\hat{g}_i(s,\mathbf{x}))ds. \qquad \textbf{[34b]}$$

We modify the decomposition Eq. **32** as follows

$$\partial_t W_1 = (\mathcal{L}-\mathcal{K}_n)W_1 - \mathcal{R}(W_1,t), \qquad \textbf{[34c]}$$

$$\partial_t \widehat{W}_2 = \mathcal{L}\widehat{W}_2 + \mathcal{K}_n W_1 + \mathcal{R}(W_1,t), \qquad \textbf{[34d]}$$

where $W_1|_{t=0} = W_0$, $\widehat{W}_2|_{t=0} = 0$. Note that $\widehat{W}_2$ solves Eq. **34d** exactly since the residual operator captures all the errors. If the error $(\partial_s-\mathcal{L})\hat{g}_i(s,\mathbf{x})$ and $\hat{g}_i(0,\mathbf{x})-\bar{g}_i$ are small, we can show that the norm of the residual operator is small in some suitable functional space by using a bootstrap argument: $||\mathcal{R}(W_1,t)||_X \le \hat{\varepsilon}\sup_{s\le t}||W_1(s)||_X$, $\hat{\varepsilon}\ll 1$. We treat $\mathcal{R}$ as a small perturbation to the stable part $\mathcal{L}-\mathcal{K}_n$ in Eq. **34c** and establish the stability for W_1.

3.6. Finite-Rank Operator in refs. 15 and 16. We construct the finite-rank operator $\mathcal{K}_n$ by approximating the commutator in Eq. **22b**, and $\mathbf{u}$ in $\mathcal{L}_{\nabla\mathbf{u}}$, $\mathcal{L}_{\mathbf{u}}$ Eq. **12** similar to Eq. **23**. Since the integral in $\mathcal{B}_C(f)(\mathbf{x}_{ij})$ Eq. **22b** is singular, we replace $\mathcal{B}_C(f)(\mathbf{x}_{ij})$ in Eq. **23** by a nonsingular version of $\mathcal{B}_C(f)(x_{ij})$, where we remove a small region near the singularity $\mathbf{y}=\mathbf{x}_{ij}$ in the integral Eq. **22b**. This adjustment provides a better overall approximation. Moreover, we perform a low rank perturbation so that the vanishing order $W_1 = O(|\mathbf{x}|^3)$ is preserved at $\mathbf{x}=0$ in Eq. **34c**, which allows us to choose a more singular weight for weighted estimates in Section 3.2.1, i.e., smaller α_f in Eq. **26**; see, e.g., $\alpha_{\omega,\eta,\xi} = (-2.9,-3,-3)$ in Eq. **29**. See more details on the constructions in sections 4.2 and 4.3 in ref. 15.

3.7. Anisotropic Flow. Due to the flow direction of $\bar{\mathbf{u}}$, the outflow property Eq. **13c** is much stronger in the y-direction than in the x-direction. This allows us to obtain sharper stability estimates in $\mathbb{R}^2_+$ away from the boundary and better control of ξ compared to η (see the damping terms in Eqs. **28a** and **28b**). Thus, we can focus the stability analysis on the coupling between ω and η in Eqs. **12a** and **12b**, formally neglecting the leading-order coupling to ξ. Moreover, the finite-rank perturbation method from Section 3.5.1 only needs to be applied near the boundary to approximate nonlocal terms such as $\mathcal{B}_C$ in Eq. **22b**. We can also use a single cutoff function with $O(1)$ support in the y (or x_2) direction-i.e., setting $N=0$ and $j=0$ in the summation in Eq. **23**-which significantly reduces the rank n of $\mathcal{K}_n$ in Eqs. **25** and **32a**.

3.7.1. Nonlinear stability. We treat the nonlinear terms Eq. **4** perturbatively and bound them by CE^2, where E is the energy. It is important to note that the stability constants, e.g., λ, C in Eq. **5**, are not sensitive to ε. Suppose that using a numerical method, we observe that the solution converges to a nontrivial steady state, and construct two approximate steady states $\bar{W}_{\varepsilon_i} = (\bar{\omega}_i,\bar{\theta}_i,\bar{c}_{l,i},\bar{c}_{\omega,i})$ with a residual error ε_i $(i=1,2)$. We expect that these profiles are ε_i close to the actual steady state $(\bar{\omega},\bar{\theta},\bar{c}_l,\bar{c}_\omega)$ (which we do not know) in some suitable spaces.[**] Then the constants in the stability estimates based on these two different profiles will be nearly identical. For example, we expect the following estimates for the terms $\bar{u}_x\eta$ in Eq. **12b**

$$|u_x(\bar{\omega}_1)\eta - u_x(\bar{\omega}_2)\eta| \lesssim (\varepsilon_1+\varepsilon_2)|\eta|.$$

Thus, we can first perform stability estimates using a profile with a residual error that does not need to be extremely small and may not satisfy Eq. **5b**. After we determine λ, C, we refine the construction of the profile and verify the constraint Eq. **5b** a-posteriori.

3.7.2. Computer-assisted estimates. We summarize key steps involving computer assistance.

1. We construct the approximate profile and estimate the profile and the residual error using numerical methods. See Section 4.
2. We approximate the more regular nonlocal part, e.g., $\mathcal{B}_C$, by a finite-rank operator $\mathcal{K}_n$. To bound the approximation error-such as constants in the estimate of $\mathcal{B}_C(f)-\mathcal{K}_{MN}(f)$ Eq. **24**-we evaluate certain integrals using numerical quadrature. See Section 4.3.
3. We track the constants in the stability estimates, which depend on the approximate profile, and compute sharp bounds with computer assistance.
4. For the finite-rank perturbation, we numerically construct the approximate solution to Eq. **33** using PDE solvers. See further discussion in Section 3.5.1.

[**] This property holds if the linearized operator around the exact steady state is invertible.

Downloaded from https://www.pnas.org by Thomas Y.Z. Hou on June 27, 2025 from IP address 162.204.127.207.

5. We track discretization and round-off errors for rigorous numerics. Discretization error is analyzed using numerical analysis [Section 4.2, (16, section 3.6 and appendix C)], while round-off error is tracked via basic interval arithmetic (41). Both are treated as small perturbations in the energy estimates Eq. **5**.

In summary, we leverage the anisotropic structure (Section 3.5.1) to reduce the rank n of $\mathcal{K}_n$ in Eqs. **25** and **32a**; control the approximation error in step 2 to improve λ and reduce n; track constants to refine bounds on λ and C in Eq. **5**; and estimate $\mathcal{K}_n$ via the methods in Section 3.5.1. These steps, combined with analytic techniques from Sections 3.2.1–3.4.2, allow us to close the nonlinear stability estimate Eq. **5**.

4. Profile and Some Rigorous Numerics

In this section, we discuss constructing the approximate steady state to Eq. **9** and some rigorous numerics. The profile's multidimensional nature requires solving a nonlocal, nonlinear PDE in 2D, posing an essential difficulty. To the best of our knowledge, the profile in the Hou–Luo scenario is the first truly multidimensional approximate self-similar blowup profile with sufficient regularity found for fluid equations.

4.1. Numerical Construction. Due to the symmetry of $\omega(x,y), \theta(x,y)$ in x, we only need to focus on $(x,y) \in \mathbb{R}^2_+$. We represent the profile as follows

$$\begin{aligned} \bar{\omega} &= \bar{\omega}_1 + \bar{\omega}_2, \quad \bar{\omega}_1 = \chi(r) r^{\alpha} \bar{g}_1(\beta), \\ \bar{\theta} &= \bar{\theta}_1 + \bar{\theta}_2, \quad \bar{\theta}_1 = \chi(r) r^{1+2\alpha} \bar{g}_2(\beta), \end{aligned} \tag{35}$$

where $r = |(x,y)|, \beta = \arctan(y/x) \in [0,\pi]$ denotes the polar coordinate in $\mathbb{R}^2_+$, $\bar{\omega}_2, \bar{\theta}_2$ capture the profile in the near field, and the semianalytic part $\bar{\omega}_1, \bar{\theta}_1$ capture the far-field behavior. Here, χ is some cutoff function with $\chi = 0$ near 0 and $\chi = 1$ in the far-field. Functions $\bar{g}_1(\beta), \bar{g}_2(\beta)$ are the angular parts of the profiles $\bar{\omega}, \bar{\theta}$ in the far-field, which cannot be determined a-priori. We represent $(\bar{\omega}_2, \bar{\theta}_2)$ in a domain $[0,L]^2$ with $L \approx 10^{13}$ using a piecewise 6-th order B-spline in x and y,

$$\bar{\omega}_2 = \sum_{i,j} a_{i,j} B_i(x) B_j(y), \tag{36}$$

where $B_i(x)$ is the B-spline basis (see ref. 16, appendix C.1). We represent $\bar{\theta}$ similarly. To construct $\mathbf{u} = \nabla^{\perp}(-\Delta)^{-1}\omega$ Eq. **9**, we solve the Poisson equation $-\Delta\phi = \omega$ to obtain ϕ using a B-spline based finite element method and then obtain $\mathbf{u} = \nabla^{\perp}\phi$.

To determine the profiles, we first solve Eqs. **9** and **10** numerically for a long enough time using the representation Eqs. **35** and **36** with time-dependent coefficients $a_{ij}(t)$ and without the semianalytic part, i.e., setting $\bar{\omega}_1 = \bar{\theta}_1 = 0$, to obtain an approximate steady state $(\bar{\omega}^{(2)}, \bar{\theta}^{(2)}, \bar{c}_{\omega}^{(1)}, \bar{c}_l^{(1)})$. We obtain the decay rate $\alpha = \bar{c}_{\omega}^{(1)}/\bar{c}_l^{(1)}$ in Eq. **35** by matching the slowest decaying parts in Eq. **9**

$$\begin{aligned} c_l r \partial_r \omega(r,\beta) &= c_{\omega}\omega + \theta_x + l.o.t., \\ c_l r \partial_r \theta(r,\beta) &= (2c_{\omega} + c_l)\theta + l.o.t., \end{aligned}$$

and use the far-field of $(\bar{\omega}^{(2)}, \bar{\theta}^{(2)})$ and curve fitting to determine $\bar{g}_1, \bar{g}_2$ in Eq. **35**. After we construct $(\bar{\omega}_1, \bar{\theta}_1)$, we fix it and refine the computation of $(\bar{\omega}_2, \bar{\theta}_2, \bar{c}_{\omega}, \bar{c}_l)$ by solving Eqs. **9** and **10** numerically using the representation Eqs. **35** and **36**. Using Eqs. **35** and **36**, we can evaluate the profile at any $\mathbf{x}$. See more details in 15, section 7, (16, appendix C.1).

4.2. Rigorous Estimates of Profile and Error. We use numerical analysis to estimate the profile and residual error. For example, to obtain a tight piecewise bound of a function f in $D_{ij} \equiv [x_i, x_{i+1}] \times [y_j, y_{j+1}]$, we have

$$\begin{aligned} \max_{x,y\in D_{ij}} |f(x,y)| \le \max_{i,j=1,2} |f(x_i, y_j| \\ + \frac{h_1^2}{8} ||\partial_x^2 f||_{L^{\infty}(D_{ij})} + \frac{h_2^2}{8} ||\partial_y^2 f||_{L^{\infty}(D_{ij})}, \end{aligned} \tag{37}$$

where $h_1 = x_{i+1} - x_i$ and $h_2 = y_{j+1} - y_j$. If f is a polynomial, e.g., $\bar{\omega}_2$ in Eq. **36**, the high-order derivatives vanish. Since we can evaluate the grid point values $f(x_i, y_j)$ using the representation formula, we can recursively use Eq. **37** to estimate the derivatives from high order to low order. For the semianalytic parts $\bar{\omega}_1, \bar{\theta}_1$ in Eq. **35** and other functions, we first obtain a rough estimate on higher-order derivatives. Then we refine the piecewise bounds using Eq. **37** by subpartitioning the domain with smaller mesh h_i.

For effective estimates without requiring too small h_i, we use higher-order error estimates based on the Lagrange, Newton, and Hermite interpolations.

4.2.1. Estimate in the far-field. For very large $|x|$, we have $\bar{\omega}_2 = \bar{\theta}_2 = 0$, $\chi(r) = 1$, and $\bar{\omega} = r^{\alpha}\bar{g}_1$, $\bar{\theta} = r^{1+2\alpha}\bar{g}_2$ Eq. **35**. We estimate $\bar{g}_i(\beta)$ with $\beta \in [0,\pi]$ using the 1D version of Eq. **37**. Since r^{γ} is monotonic, its estimates are straightforward. We then obtain piecewise bounds for $r^{\gamma}\bar{g}_i(\beta)$, $\gamma = \alpha, 1+2\alpha$, in polar coordinates, which can be transferred to the (x,y) coordinates via a covering argument. To verify inequalities in the far-field, e.g., Eq. **13c**, we factor out the decay rate r^k for some k and verify inequalities in the angular variable.

4.3. Estimate Approximation Error. We use a numerical quadrature to estimate the approximation error for the more regular terms.

We focus on a more regular nonlocal term $\mathbf{u}$ in Eq. **12** to illustrate the ideas. Let $\hat{\mathbf{u}}(\omega)$ be the finite-rank approximation of $\mathbf{u}$ and ρ be a singular weight like φ defined in Eq. **19** in the energy estimates. We rewrite the error $\rho(\mathbf{x})(\mathbf{u}(\omega) - \hat{\mathbf{u}}(\omega))$ as an integral of ω: $I(\mathbf{x}) = \rho(\mathbf{x}) \int K(\mathbf{x},\mathbf{y})\omega(\mathbf{y})d\mathbf{y}$, and bound it using the weighted norm $||\omega\rho||_{L^{\infty}}$. For example, the kernel associated with $\mathbf{u}$ is $K(\mathbf{z}) = \frac{1}{2\pi}\nabla^{\perp}\log|\mathbf{z}|$. To obtain a sharp estimate, we symmetrize the integral and estimate $I(\mathbf{x}) = \rho(\mathbf{x}) \int_{y_i \ge 0} K^{\mathrm{sym}}(\mathbf{x},\mathbf{y})\omega(\mathbf{y})d\mathbf{y}$ with the symmetrized kernel K^{sym}. We have two singularities in $I(\mathbf{x})$: the singularity of $\rho(\mathbf{x})$ near $\mathbf{x} = 0$ and the singularity at $\mathbf{x} = \mathbf{y}$ in the kernel $K(\mathbf{x},\mathbf{y})$.

In the case without an approximation, we get $K^{\mathrm{sym}}(\lambda\mathbf{x}, \lambda\mathbf{y}) = \lambda^{-1}K^{\mathrm{sym}}(\mathbf{x},\mathbf{y})$ for the kernel of $\mathbf{u}$ with -1 homogeneity. Changing $\mathbf{y} = \lambda\hat{\mathbf{y}}, \mathbf{x} = \lambda\hat{\mathbf{x}}$ gives

$$\begin{aligned} I(x) &= \rho(\mathbf{x}) \int_{\mathbb{R}^2_{++}} K^{\mathrm{sym}}(\mathbf{x},\mathbf{y})\omega(\mathbf{y})d\mathbf{y} \\ &= \rho(\lambda\hat{\mathbf{x}}) \int_{\mathbb{R}^2_{++}} K^{\mathrm{sym}}(\lambda\hat{\mathbf{x}}, \lambda\hat{\mathbf{y}})\omega(\lambda\hat{\mathbf{y}})\lambda^2 d\hat{\mathbf{y}} \\ &= \lambda\rho_{\lambda}(\hat{\mathbf{x}}) \int_{\mathbb{R}^2_{++}} K^{\mathrm{sym}}(\hat{\mathbf{x}},\hat{\mathbf{y}})\omega_{\lambda}(\hat{\mathbf{y}})d\hat{\mathbf{y}}, \end{aligned}$$

Downloaded from https://www.pnas.org by Thomas Y.Z. Hou on June 27, 2025 from IP address 162.204.127.207.

where $f_\lambda(\mathbf{x}) = f(\lambda\mathbf{x})$. We bound it using $||\omega\rho||_{L^\infty}$:

$$|I(x)| \le \lambda ||\omega_\lambda \rho_\lambda||_{L^\infty} \rho_\lambda(\hat{\mathbf{x}}) \int_{\mathbb{R}^2_{++}} |K^{\mathrm{sym}}(\hat{\mathbf{x}}, \hat{\mathbf{y}})| \frac{1}{\rho_\lambda(\hat{\mathbf{y}})} d\hat{\mathbf{y}}.$$

Since $||\omega_\lambda \rho_\lambda||_{L^\infty} = ||\omega\rho||_{L^\infty}$, it suffices to compute the rescaled integral. By choosing λ adaptive to $\mathbf{x}$, e.g. $\lambda \asymp |\mathbf{x}|/|\hat{\mathbf{x}}|$ with $|\hat{\mathbf{x}}| \asymp 1$, the singularity $\hat{\mathbf{y}} = \hat{\mathbf{x}}$ in the kernel is restricted to some finite domain away from the origin. Moreover, the integrand is locally integrable. Thus, we can design an adaptive mesh dense in the $O(1)$ region to compute the integrals. In the case with an approximation term such as $\hat{u}(\omega)$, we can apply a similar rescaling argument to bound the integrals. For more details, see ref. 16, section 4.

Data, Materials, and Software Availability. There are no data underlying this work.

ACKNOWLEDGMENTS. The work of J.C. was in part supported by the NSF Grant DMS-2408098. The research of T.Y.H. was in part supported by NSF Grant DMS-2205590 and the Choi Family Gift Fund. We would like to thank Russel E. Caflisch, Javier Gómez-Serrano, Vladimir Sverak, and Terence C. Tao for many constructive comments and suggestions for the original manuscript, which greatly improve the quality of our paper.

1. A. Majda, A. Bertozzi, *Vorticity and Incompressible Flow* (Cambridge University Press, 2002), vol. 27.
2. A. Kiselev, "Small scales and singularity formation in fluid dynamics" in *Proceedings of the International Congress of Mathematicians* (World Scientific Publishing, 2018).
3. G. Luo, T. Y. Hou, Potentially singular solutions of the 3D axisymmetric Euler equations. *Proc. Natl. Acad. Sci. U.S.A.* **111**, 12968–12973 (2014).
4. G. Luo, T. Hou, Toward the finite-time blowup of the 3D incompressible Euler equations: A numerical investigation. *SIAM Multiscale Model. Simul.* **12**, 1722–1776 (2014).
5. M. Sherman, *Computer Proof 'Blows Up' Centuries-Old Fluid Equations* (Quanta Magazine, 2022), https://www.quantamagazine.org/computer-helps-prove-long-sought-fluid-equation-singularity-20221116/.
6. P. Constantin, C. Fefferman, A. Majda, Geometric constraints on potentially singular solutions for the 3D Euler equations. *Comm. Partial Differ. Equ.* **21**, 559–571 (1996).
7. J. Deng, T. Hou, X. Yu, Geometric properties and nonblowup of 3D incompressible Euler flow. *Comm. Partial Differ. Equ.* **30**, 225–243 (2005).
8. D. Barkley, A fluid mechanic's analysis of the teacup singularity. *Proc. R. Soc. A* **476**, 2020348 (2020).
9. A. Kiselev, V. Sverak, Small scale creation for solutions of the incompressible two dimensional Euler equation. *Ann. Math.* **180**, 1205–1220 (2014).
10. K. Choi *et al.*, On the finite-time blowup of a 1D model for the 3D axisymmetric Euler equations. *CPAM* **70**, 2218–2243 (2017).
11. A. Kiselev, L. Ryzhik, Y. Yao, A. Zlatos, Finite time singularity for the modified SQG patch equation. *Ann. Math.* **184**, 909–948 (2016).
12. K. Choi, A. Kiselev, Y. Yao, Finite time blow up for a 1D model of 2D Boussinesq system. *Comm. Math. Phys.* **334**, 1667–1679 (2015).
13. J. Chen, T. Y. Hou, Finite time blowup of 2D Boussinesq and 3D Euler equations with $C^{1,\alpha}$ velocity and boundary. *Comm. Math. Phys.* **383**, 1559–1667 (2021).
14. Y. Wang, C. Y. Lai, J. Gomez-Serrano, T. Buckmaster, Asymptotic self-similar blow-up profile for three-dimensional axisymmetric Euler equations using neural networks. *Phys. Rev. Lett* **130**, 244002 (2023).
15. J. Chen, T. Y. Hou, Stable nearly self-similar blowup of the 2D Boussinesq and 3D Euler equations with smooth data I: Analysis. arXiv [Preprint] (2022). http://arxiv.org/abs/2210.07191v3 (Accessed 9 May 2023).
16. J. Chen, T. Y. Hou, Stable nearly self-similar blowup of the 2D Boussinesq and 3D Euler equations with smooth data II: Rigorous numerics. *MMS* **23**, 25–130 (2025).
17. T. M. Elgindi, Finite-time singularity formation for $C^{1,\alpha}$ solutions to the incompressible Euler equations on $\mathbb{R}^3$. *Ann. Math.* **194**, 647–727 (2021).
18. T. M. Elgindi, T. E. Ghoul, N. Masmoudi, On the stability of self-similar blow-up for $C^{1,\alpha}$ solutions to the incompressible Euler equations on $\mathbb{R}^3$. *Camb. J. Math.* **9**, 647–727 (2021).
19. T. M. Elgindi, F. Pasqualotto, From instability to singularity formation in incompressible fluids. arXiv [Preprint] (2023). http://arxiv.org/abs/2310.19780 (Accessed 30 October 2023).
20. D. Cordoba, L. Martinez-Zoroa, F. Zheng, Finite time singularities to the 3D incompressible Euler equations for solutions in $C^{1,\alpha} \cap C^\infty(R^3 \backslash 0) \cap L^2$. arXiv [Preprint] (2023). http://arxiv.org/abs/2308.12197 (Accessed 23 August 2023).
21. D. Córdoba, L. Martínez-Zoroa, Blow-up for the incompressible 3D-Euler equations with uniform $C^{1,1/2-\epsilon} \cap l^2$ force. arXiv [Preprint] (2023). http://arxiv.org/abs/2309.08495 (Accessed 15 September 2023).
22. T. Hou, Z. Lei, On the stabilizing effect of convection in three-dimensional incompressible flows. *Commun. Pure Appl. Math.* **62**, 501–564 (2009).
23. J. Chen, On the regularity of the De gregorio model for the 3D Euler equations. *J. Eur. Math. Soc.* **1399**, 1–59 (2023).
24. F. Merle, P. Raphaël, I. Rodnianski, J. Szeftel, On blow up for the energy super critical defocusing nonlinear Schrödinger equations. *Invent. Math.* **227**, 247–413 (2022).
25. F. Merle, P. Raphaël, I. Rodnianski, J. Szeftel, On the implosion of a compressible fluid I: Smooth self-similar inviscid profile. *Ann. Math.* **2**, 567–778 (2022).
26. C. Collot, T. Ghoul, N. Masmoudi, V. T. Nguyen, Refined description and stability for singular solutions of the 2D Keller-Segel system. *Commun. Pure Appl. Math.* **75**, 1419–1516 (2022).
27. J. Chen, T. Y. Hou, D. Huang, Asymptotically self-similar blowup of the Hou-Luo model for the 3D Euler equations. *Ann. PDE* **8**, 24 (2022).
28. D. W. McLaughlin, G. C. Papanicolaou, C. Sulem, P. L. Sulem, Focusing singularity of the cubic Schrödinger equation. *Phys. Rev. A* **34**, 1200 (1986).
29. C. E. Kenig, F. Merle, Global well-posedness, scattering and blow-up for the energy-critical, focusing, non-linear Schrödinger equation in the radial case. *Invent. Math.* **166**, 645–675 (2006).
30. J. Chen, T. Y. Hou, D. Huang, On the finite time blowup of the De Gregorio model for the 3D Euler equations. *Commun. Pure Appl. Math.* **74**, 1282–1350 (2021).
31. F. Merle, P. Raphaël, I. Rodnianski, J. Szeftel, On the implosion of a compressible fluid II: Singularity formation. *Ann. Math.* **2**, 779–889 (2022).
32. J. Chen, G. Cialdea, S. Shkoller, V. Vicol, Vorticity blowup in 2D compressible Euler equations. arXiv [Preprint] (2024). http://arxiv.org/abs/2407.06455 (Accessed 8 July 2024).
33. J. Chen, Vorticity blowup in compressible Euler equations in $\mathbb{R}^d$, $d \ge 3$. arXiv [Preprint] (2024). http://arxiv.org/abs/2408.04319 (Accessed 8 August 2024).
34. T. Buckmaster, G. Cao-Labora, J. Gómez-Serrano, Smooth imploding solutions for 3D compressible fluids, *Forum Math. Pi.* **13**, e6 (2025).
35. C. Collot, T. E. Ghoul, N. Masmoudi, Singularity formation for Burgers' equation with transverse viscosity. *Ann. Sci. Éc. Norm. Supér.* **4**, 1047–1133 (2022).
36. P. Liu, "Spatial profiles in the singular solutions of the 3D Euler equations and simplified models," PhD thesis, California Institute of Technology (2017).
37. J. Sherman, W. J. Morrison, Adjustment of an inverse matrix corresponding to a change in one element of a given matrix. *Ann. Math. Stat.* **21**, 124–127 (1950).
38. G. David, J. L. Journé, A boundedness criterion for generalized Calderón-Zygmund operators. *Ann. Math.* **120**, 371–397 (1984).
39. A. McIntosh, Algèbres d'opérateurs définis par des intégrales singulières. *CR Acad. Sci. Paris Sér. I Math.* **301**, 395–397 (1985).
40. G. David, J. L. Journé, S. Semmes, Opérateurs de Calderón-Zygmund, fonctions para-accrétives et interpolation. *Revista Matemática Iberoamericana* **1**, 1–56 (1985).
41. S. M. Rump, Verification methods: Rigorous results using floating-point arithmetic. *Acta Numer.* **19**, 287–449 (2010).

Downloaded from https://www.pnas.org by Thomas Y.Z. Hou on June 27, 2025 from IP address 162.204.127.207.